Supplementary Information

Strong non-Arrhenius behavior at low temperatures in the OH + HCl → H_2O + Cl reaction due to resonance induced quantum tunneling

Xin Xu, Jun Chen, Xiaoxiao Lu, Wei Fang, Shu Liu, and Dong H. Zhang*

Supplementary Methods

A. Potential energy surface

The potential energy surface (PES) of HCl+OH system was constructed using explicitly correlated unrestricted coupled cluster theory with singles, doubles, and perturbative triples[1, 2](UCCSD(T)-F12b/UCCSD(T)-F12a), together with the aug-cc-pVTZ basis sets. The spin-orbit coupling of both OH reagent and Cl product channels calculated at MRCI/aug-cc-pVTZ level of theory. The CASSCF wave-function with an active space of (5e, 3o) was used as reference for MRCI. All these calculations were performed with the MOLPRO 2012.1 package.[3]

The fundamental invariant neural network (FI-NN) can approximate any function to arbitrary accuracy[4]. Because FI-NN minimizes the size of input permutation invariant polynomials, it can efficiently reduce the evaluation time of potential energy, in particular for polyatomic systems. In this work, we employed the FI-NN functions to fit the PES. An iteratively geometry selection scheme[5] based on the combination of FI-NN fittings and trajectory calculations was used to fully sample the space. In this work, the PES was fitted with NN functions containing two hidden layers, which have the following functional form:

$$y = b^3 + \sum_{k=1}^{K} w_k^3 \cdot f^2\left[b_k^2 + \sum_{j=1}^{J} w_{jk}^2 \cdot f^1\left(b_j^1 + \sum_{i=1}^{I} w_{ij}^1 \cdot x_i \right) \right] \text{*}$$

MERGEFORMAT (1)

in which, x_i is the input vector, corresponding to the coordinates, and y is the output

of NN function, corresponding to the potential energy. The structure can be noted as *I-J-K-1*. For neurons in hidden layers and output layer, the input value of a neuron is the weighted sum of outputs from the previous layer, plus a bias b_i^1, b_j^2 or b^3. Connected with neighbouring layers are the weights $w_{i,j}^1$, $w_{j,k}^2$ and w_k^3. In each neuron the input is transformed by an excitation function, here we use the hyperbolic tangent function *tanh* for f^1 and f^2 in hidden layers and linear function for output layer. The Levenberg-Marquardt algorithm[6] was used to iteratively adjust the parameters of NN function to decrease RMSE, and the "early stoping" method[7] was used to avoid over fitting. The quality of PES fitting was indicated by the root mean square error (RMSE) defined as:

$$\mathrm{RMSE} = \sqrt{\frac{1}{N}\sum_{n=1}^{N}\left(E_n^{ab\ initio} - E_n^{fit}\right)^2} \quad \backslash\text{* MERGEFORMAT (2)}$$

More than 70,000 points were used to construct the PESs using the neural networks. These points, covering the asymptotic reactive channels of HCl+OH, Cl+H_2O, as well as interaction region, were selected iteratively by an effective scheme which was proposed for high dimensional PES constructions. For the spin-orbit coupling, 38000 points were used for fitting in total. The 7 fundamental invariants (FIs) are used for the input layer. The asymptotic channels and interaction region were fitted segmentally to improve the fitting accuracy and efficiency, and connected with smooth switch functions. The switch functions for each part are defined from the bond distances between Cl and H atoms as (with H atoms sorted to satisfy $r\mathrm{Cl{-}H_1} \leqslant r\mathrm{Cl{-}H_2}$):

$$\begin{aligned}
r_1 &= \min(r_{Cl\text{-}O}, r_{Cl-H_1}, r_{Cl\text{-}H_2}) \\
r_2 &= \min(r_{H_2\text{-}Cl}, r_{H_1\text{-}O}, r_{H_1\text{-}H_2}, r_{Cl\text{-}O}) \\
w_{Cl+H_2O} &= \log sig[5.0*(r_1 - 5.0)] \qquad \backslash\text{*} \\
w_{HCl+OH} &= (1 - w_{Cl+H_2O})*\log sig[5.0*(r_2 - 5.0)] \\
w_{INT} &= 1 - w_{Cl+H_2O} - w_{HCl+OH}
\end{aligned}$$

MERGEFORMAT (3)

The final functional form of Cl+H_2O PES is written as:

$$V = V_{SO} + V_{Cl+H_2O} w_{Cl+H_2O} + V_{HCl+HO} w_{HCl+HO} + V_{INT} w_{INT}. \quad \text{* MERGEFORMAT (4)}$$

The parameters of FI-NN structures and fitting errors of each part are listed in Supplementary Table 3. Extensive trajectory and quantum scattering tests show that, with the overall fitting error 3.07 and 3.12 meV, respectively, for F12a and F12b PES, both the fitting procedure and the number of ab initio points are fully converged. The fitting error for spin-orbit coupling is 0.19 meV.

B. Initial state selected wave packet approach and numerical parameters

The coordinate systems and wavefunctions representations for diatom–diatom scattering studies are outlined here. For details, please refer Ref[8]. Figure 1 shows the reagent Jacobi coordinates (R, r_1, r_2, θ_1, θ_2, φ) for the HCl + OH diatom–diatom arrangement.

The Hamiltonian for the HCl + OH arrangement with a given total angular momentum J can be written as

$$H = -\frac{\hbar^2}{2\mu}\frac{\partial^2}{\partial R^2} + \frac{(\mathbf{J}-\mathbf{j}_{12})^2}{2\mu R^2} + \frac{\mathbf{j}_1^2}{2\mu_1 r_1^2} + \frac{\mathbf{j}_2^2}{2\mu_2 r_2^2} + V(R, r_1, r_2, \theta_1, \theta_2, \varphi) + h_1(r_1) + h_2(r_2) \quad \text{* MERGEFORMAT (5)}$$

where μ denotes the reduced mass between the center of mass of reagent HCl and OH, $\mathbf{J}$ denotes the total angular momentum operator, $\mathbf{j}_1$ and $\mathbf{j}_2$ are the rotational angular momentum operators of HCl and OH, which couples to form $\mathbf{j}_{12}$. The diatomic reference Hamiltonian $h_i(r_i)$ $(i = 1, 2)$ is defined as

$$h_i(r_i) = -\frac{\hbar^2}{2\mu_i}\frac{\partial^2}{\partial r_i^2} + V_i(r_i). \quad \text{* MERGEFORMAT (6)}$$

We expand the time-dependent wave function by direct product of the

translational basis of R, the vibrational basis $\phi_{v_i}(r_i)$, and the body-fixed (BF) rovibrational eigenfunction as

$$\Psi^{JMp}_{v_0 j_0 K_0}(\mathbf{R},\mathbf{r_1},\mathbf{r_2},t) = \sum_{n,v,j,K} F^{JMp}_{nvjK,v_0 j_0 K_0}(t) u_n^{v_1}(R)\phi_{v_1}(r_1)\phi_{v_2}(r_2)\Upsilon^{JMp}_{jK}(\hat{R},\hat{r}_1,\hat{r}_2). * \text{MERGEFORMAT (7)}$$

The BF total angular momentum eigenfunctions can be written as,

$$\Upsilon^{JMp}_{jK} = (1+\delta_{K0})^{-1/2}\sqrt{\frac{2J+1}{8\pi}}[D^{J*}_{K,M}Y^{j_{12}K}_{j_1 j_2} + p(-1)^{j_1+j_2+j_{12}+J}D^{J*}_{-K,M}Y^{j_{12}-K}_{j_1 j_2}] * \text{MERGEFORMAT (8)}$$

where $D^J_{K,M}(\Theta\Phi\Psi)$ is the Wigner rotation matrix with three Euler angles $(\Theta\Phi\Psi)$, p denotes the total parity of the system defined as $p=(-1)^{j_1+j_2+L}$, $L=J-j_{12}$ is the orbital angular momentum of AB and CD, and $Y^{j_{12}K}_{j_1 j_2}$ is the angular momentum eigenfunction of $\mathbf{j}_{12}$,

$$Y^{j_{12}K}_{j_1 j_2} = \sum_{m_1}\langle j_1 m_1 j_2 K-m_1 \mid j_{12}K\rangle y_{j_1 m_1}(\theta_1,0)y_{j_2 K-m_1}(\theta_2,\phi) * \text{MERGEFORMAT (9)}$$

where y_{jm} are spherical harmonics. From Eq. * MERGEFORMAT (9), one can see that the K = 0 block can only appear when $p(-1)^{j_1+j_2+j_{12}+J}=1$.

We construct an initial wave packet $\psi_i(0)$ and propagate it using the split-operator method. The time-independent (TI) wavefunction can be obtained by performing a Fourier transform of the time-dependent wave function as

$$\left|\psi^+_{iE}\right\rangle = \frac{1}{a_i(E)}\int_0^\infty e^{\frac{i}{\hbar}(E-H)t}\mid\psi_i(0)\rangle dt * \text{MERGEFORMAT (10)}$$

The coefficient $a_i(E)$ is the overlap between the initial wave packet and the energy-normalized asymptotic scattering function, $a_i(E)=\langle\phi_{iE}\mid\psi_i(0)\rangle$. Because the resonance wave functions are located in entrance channel, we started to perform Fourier transform after a quite long propagation time of ~1,500,000 au in order to filter elastic/inelastic components of the scattering wave function, which are much

larger in magnitude than the resonance wave functions.

The total reaction probability for that specific initial state for a whole range of energies can be obtained by evaluating the reactive flux at a dividing surface $s = s_0$

$$P^{Jp}_{v_0 j_0 K_0}(E) = \frac{\hbar}{m_s} \mathrm{Im}\left[\langle \psi^+_{iE} \mid \delta(s - s_0) \frac{\partial}{\partial s} \mid \psi^+_{iE} \rangle \right] \quad \text{* MERGEFORMAT (11)}$$

The reaction cross section for a specific initial state is obtained by summing over the reaction probabilities $P^{Jp}_{v_0 j_0 K_0}$ for all the partial waves,

$$\sigma_{v_0 j_0}(E) = \frac{1}{(2j_1+1)(2j_2+1)} \frac{\pi}{k^2} \times \sum_{JpK_0} (2J+1) P^{Jp}_{v_0 j_0 K_0}(E) \quad \text{* MERGEFORMAT (12)}$$

The initial state-specific thermal rate constant is given in terms of the total integral cross section of Eq. * MERGEFORMAT (12) by

$$k_{v_0 j_0}(T) = \left(\frac{8kT}{\pi \mu} \right) (kT)^{-2} \times \int_0^\infty dE_t E_t \exp(-E_t / kT) \sigma_{v_0 j_0}(E_t) \quad \text{* MERGEFORMAT (13)}$$

where E_t is the translational energy.

By using the uniform J-shifting approach with a temperature dependent shifting constant, all we have to do is to calculate the reaction probabilities at only a few total angular momentum values of J[9-11],

$$k_u(T) = \sqrt{\frac{2\pi}{(\mu kT)^3}} Q^0(T) \sum_J (2J+1) e^{-B(T)J(J+1)/kT} \quad \text{* MERGEFORMAT (14)}$$

$$B_i(T) = \frac{kT}{J_{i+1}(J_{i+1}+1) - J_i(J_i+1)} ln\left(\frac{Q^{J_i}}{Q^{J_{i+1}}} \right) \quad (i = 1, 2) \quad \text{* MERGEFORMAT (15)}$$

$$Q^J = \int P^J(E) e^{-E/kT} dE \quad \text{* MERGEFORMAT (16)}$$

A further approximation is to use the J-shifting (JS) approximation[12] to get the

initial state-specific rate constant, in which the reaction probabilities at nonzero total angular momentum are all calculated by simply shifting the J=0 reaction probabilities,

$$P^{J>0}(E) = P^{J=0}(E - \Delta E(J)) \quad \text{* MERGEFORMAT (17)}$$

where $\Delta E(J) = B^* J(J+1)$, the rotational constant B^*=0.223 cm^{-1} ($B^* = 1/\mu_R R^{*2}$) with R^* being the center of mass distance between OH and HCl at the saddle point.

The numerical parameters for the wave packet propagation were as follows: a total of 512 sine functions (among them 60 for the interaction region) were employed for the translational coordinate R in a range of [3.5, 42.0]a_0. Five HCl vibrational basis functions were used in the asymptotic region, while 30 were used in the interaction region to expand the wave function for r_1 going from 1.5 a_0 to 6.0 a_0. For rotational degrees of freedom, we used 60 HCl rotational states and 26 OH rotational states. The initial Gaussian wave packet was centered at 32 a_0. A dividing surface at 3.5 a_0 was used for flux analysis. The wave packet propagation was carried out using a time increment of 10 a.u.

C. Transition state wave packet approach and numerical parameters

The time-dependent transition state wave packet (TSWP) approach to the CRP N(E) was derived by Zhang and Light[12] from the famous formulation given by Miller and co-workers[13],

$$N(E) = \frac{(2\pi)^2}{2} tr[\delta(E-H)F_2\delta(E-H)F_1], \quad \text{* MERGEFORMAT (18)}$$

where the $F_i's$ are quantum flux operators at dividing surfaces (which may or may not be the same).

In the TSWP approach we first choose a dividing surface S_1 separating the products fromreactants preferably located to minimize the density of internal (transition) states for the energy region considered. Then initial wave packets $\left|\phi_i^+\right\rangle (i = 1, N)$ are constructed as the direct products of the Hamiltonian eigenstates on

S_1, $\left|\phi_i^+\right\rangle$, and flux operator eigenstate $\left|+\right\rangle$ with positive eigenvalue λ for the coordinate perpendicular to S_1, i.e.,

$$\begin{aligned} &H_{S_1}|\phi_i\rangle = \varepsilon_i|\phi_i\rangle, \\ &F|+\rangle = \lambda|+\rangle, \\ &|\phi_i^+\rangle = |\phi_i\rangle|+\rangle, \end{aligned} \qquad \text{* MERGEFORMAT (19)}$$

where the flux operator F is defined as

$$F = \frac{1}{2\mu}[\delta(q-q_0)\hat{p}_q + \hat{p}_q\delta(q-q_0)]. \text{* MERGEFORMAT (20)}$$

Here μ is the reduced mass of the system, q is the coordinate perpendicular to the dividing surface located at $q = q_0$ which separates products from reactants, and $\hat{p}_q$ is the momentum operator conjugate to the coordinate q. It is well known that in one dimension the flux operator only has a $\pm$ pair of non-vanishing eigenvalues, and the corresponding eigenstates are also complex conjugates[14-16]

After constructing the initial wave packets, we propagated them in time as in the ISSWP approach. The CRP N(E) can be computed as

$$N(E) = \sum_{i=1}^{n} N_i(E) = \sum_{i=1}^{n} \langle\psi_i(E)|F|\psi_i(E)\rangle. \text{* MERGEFORMAT (21)}$$

The energy-dependent wave functions $|\psi_i(E)\rangle$ are calculated on *the second dividing surface* as

$$\psi_i(E) = \sqrt{\lambda}\int_{-\infty}^{+\infty} dt e^{i(E-H)t}|\phi_i^+\rangle. \quad \text{* MERGEFORMAT (22)}$$

Applying to the HCl+OH reaction, the Hamiltonian in mass-scaled Jacobi coordinates can be written as[17, 18]

$$H = \frac{1}{2\mu}\sum_{i=1}^{3}\left(-\frac{\partial^2}{\partial s_i^2} + \frac{j_i^2}{s_i^2}\right) + V(s_1, s_2, s_3, \theta_1, \theta_2, \phi), \text{* MERGEFORMAT (23)}$$

Where j_1 and j_2 are the rotational angular momenta of HCl and OH, which are coupled to form j_{12}. In the body-fixed frame the orbital angular momentum j_3 is represented as $(J-j_{12})^2$, and J is the total angular momentum. In Eq. * MERGEFORMAT (23), μ is the mass of the system,

$$\mu=(\mu_1\mu_2\mu_3)^{1/3}, \qquad \text{* MERGEFORMAT (24)}$$

with μ_i being the reduced massed for HCl, OH, and the system,

$$\begin{aligned}\mu_1&=\frac{m_H m_H}{m_H+m_H},\\ \mu_2&=\frac{m_H m_O}{m_H+m_O},\\ \mu_3&=\frac{(m_H+m_H)(m_H+m_O)}{m_H+m_H+m_H+m_O}.\end{aligned} \qquad \text{* MERGEFORMAT (25)}$$

The mass-scaled coordinates s_i are defined as

$$s_i^2=\frac{\mu_i}{\mu}R_i^2, \qquad \text{* MERGEFORMAT (26)}$$

where $R_i(i=1-3)$ are the bond lengths for HCl, OH, and the intermolecular distance between the centers of mass of HCl and OH, respectively.

The coupled angular momentum basis sets used to expand the TD wavefunction under body-fixed frame are defined as

$$y_{jK}^{JMp}=(1+\delta_{K0})^{-1/2}\sqrt{\frac{2J+1}{8\pi}}[D_{KM}^{J}Y_{j_1j_2}^{j_{12}K}+p(-1)^{j_1+j_2+j_{12}+J}D_{-KM}^{J}Y_{j_1j_2}^{j_{12}-K}], \text{*}$$

MERGEFORMAT (27)

where D_{KM}^{J} is the Wigner rotation matrix, p is the parity of the system, K is the projection of total angular momentum on the body-fixed axis, and $Y_{j_1j_2}^{j_{12}K}$ is the angular momentum eigenfunction of j_{12},

$$Y_{j_1j_2}^{j_{12}K}=\sum_{m_1}\langle j_1m_1j_2K-m_1\mid j_{12}K\rangle y_{j_1m_1}(\theta_1,0)y_{j_2K-m_1}(\theta_2,\phi) \text{*}$$

MERGEFORMAT (28)

where y_{jm} are spherical harmonics. Note that in Eq. * MERGEFORMAT (27), the

restriction $p(-1)^{j_1+j_2+j_{12}+J}=1$ for $K=0$ partitions the whole rotational basis set into even and odd parities. Thus a $K=0$ initial state can only appear in one of these two parity blocks.

For the convenient of choosing the dividing surface S_1, we define two new "reaction coordinate" variables q_1 and q_3 by translating and rotating the s_1 and s_3 axes,

$$\begin{pmatrix} q_1 \\ q_3 \end{pmatrix} = \begin{pmatrix} cos\chi & sin\chi \\ -sin\chi & cos\chi \end{pmatrix} \begin{pmatrix} s_1 - s_1^0 \\ s_3 - s_3^0 \end{pmatrix}. \quad \text{* MERGEFORMAT (29)}$$

The Hamiltonian in Eq. * MERGEFORMAT (23) can be rewritten as

$$H = \frac{1}{2\mu}\left(-\frac{\partial^2}{\partial q_1^2} - \frac{\partial^2}{\partial s_2^2} - \frac{\partial^2}{\partial q_3^2} + \frac{j_1^2}{s_1(q_1, q_3, s_1^0, s_3^0)^2} + \frac{j_2^2}{s_2^2} + \frac{j_3^2}{s_3(q_1, q_3, s_1^0, s_3^0)^2}\right) + V. \quad \text{* MERGEFORMAT (3}$$

Generally, we can choose the dividing surface S_1 at $q_1 = 0$ by changing s_1^0, s_3^0 and χ, construct the initial wave packets in $(q_1, s_2, q_3, \theta_1, \theta_2, \phi)$ coordinates, then transfer them to the $(s_1, s_2, s_3, \theta_1, \theta_2, \phi)$ coordinates and propagate them to generate $\psi_i(E)$ and $N(E)$.

The contributions of individual K_0 to thermal rate constants can be obtained from the CRP via the Boltzmann average

$$k(K_0, T) = \frac{1}{2\pi Q_r(T)} \sum_J (2J+1) \int_0^\infty dE e^{-E/k_B T} N(J, K_0, E) \quad \text{*}$$

MERGEFORMAT (31)

where k_B is the Boltzmann constant, T is the temperature, $Q_r(T)$ is the reactant partition function. The electronic partition function $Q_{elec}(T)$ can be calculated as

$$Q_{elec}(T) = (1 + e^{-\Delta E/kT}), \qquad \text{* MERGEFORMAT (32)}$$

Under the J-K shifting approximation the thermal rate constant can be obtained from $N^{J=0}(E)$ as

$$k(T) = \frac{Q_{rot}^{TS}}{2\pi Q_r(T)} \int_0^\infty dE e^{-e/KT} N^{J=0}(E) \quad \text{*} \quad \text{MERGEFORMAT}$$

(33)

where Q_{rot}^{TS} is the rotational partition function for the complex at the transition state point.

The numerical parameters used in the current study are as follows: We used a total number of 512 sine functions (among them 60 for the interaction region) for the translational coordinate s_3 in a range of [3.5,42.0] a_0. A total of 30 vibrational functions are employed for s_1 in the range of [1.5,6.0] a_0 for the reagents HCl. Here, we employed the potential-averaged five-dimensional (PA5D)[8, 19] to get converged reaction probabilities for collision energy up to 0.4 eV. For the rotational basis, we used j_{1max}= 60 for HCl and j_{2max}= 26 for OH. The values of s_1^0, s_3^0 and χ which define the transition state surface were carefully chosen to be 4.8 a_0, 2.68 a_0 and 3.5° to minimize the density of states on the dividing surface. The vibrational eigenfunctions on the first dividing surface were solved using the same basis sets as described above. A total number of 300 transition states were used in order to obtain a well converged CRP. We propagated the wave packets for 40000 a.u. of time with a time step of 10 to converge the low energy CRP at the second dividing surface located at s1= 3.5 a_0.

Supplementary Table 1 Optimized geometries of the stationary points for the HCl + OH→Cl + H_2O reaction. Distances and angles are in units of bohr and degree, respectively.

Species	Method	R_{HO}	$R_{OH'}$	$R_{H'Cl}$	$\theta_{HOH'}$	$\theta_{OH'Cl}$	$\phi_{HOH'Cl}$	E
HO + HCl	F12a PES[a]	1.834		2.413				0.0
	F12a-so PES[b]	1.834		2.413				0.0
	F12b PES[c]	1.834		2.413				0.0
	F12b-so PES[d]	1.834		2.413				0.0
	ZZGX PES [e]	1.833		2.413				0.0
	AVTZ/UCCSD(T)-F12a[f]	1.834		2.413				0.0
	AVTZ/UCCSD(T)-F12b[g]	1.834		2.413				0.0
RC (HO···HCl)	F12a PES[a]	1.837	3.889	2.428	112.8	175.4	0.0	-0.155
	F12a-so PES[b]	1.837	3.889	2.428	113.1	175.4	0.0	-0.148
	F12b PES[c]	1.836	3.872	2.428	112.7	174.4	0.0	-0.154
	F12b-so PES[d]	1.836	3.873	2.427	113.0	174.4	0.0	-0.147
	ZZGX PES [e]	1.836	3.908	2.427	116.1	176.6	0.0	-0.152
	AVTZ/UCCSD(T)-F12a[f]	1.836	3.869	2.429	112.8	174.3	0.0	-0.155

	AVTZ/UCCSD(T)-F12b[g]	1.836	3.871	2.429	112.8	174.2	0.0	-0.155
TS	F12a PES[a]	1.837	2.541	2.619	102.6	144.8	52.8	0.088
	F12a-so PES[b]	1.837	2.541	2.619	102.6	144.9	52.8	0.095
	F12b PES[c]	1.838	2.528	2.623	102.6	146.2	51.0	0.097
	F12b-so PES[d]	1.838	2.529	2.623	102.6	146.6	51.0	0.104
	ZZGX PES [e]	1.838	2.522	2.626	102.3	143.0	60.3	0.095
	AVTZ/UCCSD(T)-F12a[f]	1.837	2.516	2.627	102.5	144.3	55.9	0.090
	AVTZ/UCCSD(T)-F12b[g]	1.837	2.511	2.629	102.5	144.0	56.4	0.096
PC ($H_2O\cdots Cl$)	F12a PES[a]	1.817	1.817	5.402	104.7	63.8	98.7	-0.957
	F12a-so PES[b]	1.816	1.816	5.419	104.7	63.8	98.8	-0.953
	F12b PES[c]	1.816	1.816	5.400	104.8	64.1	98.3	-0.953
	F12b-so PES[d]	1.816	1.816	5.418	104.7	64.1	98.5	-0.949
	ZZGX PES [e]	1.816	1.816	5.421	104.7	63.9	98.8	-0.953
	AVTZ/UCCSD(T)-F12a[f]	1.818	1.817	5.405	104.8	64.0	98.6	-0.957
	AVTZ/UCCSD(T)-F12b[g]	1.816	1.816	5.406	104.8	63.9	98.6	-0.953
H_2O+Cl	F12a PES[a]	1.812	1.812	104.5				-0.800
	F12a-so PES[b]	1.812	1.812	104.5				-0.826
	F12b PES[c]	1.812	1.812	104.4				-0.800
	F12b-so PES[d]	1.812	1.812	104.4				-0.822
	ZZGX PES [e]	1.816	1.811	104.1				-0.794
	AVTZ/UCCSD(T)-F12a[f]	1.812	1.812		104.5			-0.800
	AVTZ/UCCSD(T)-F12b[g]	1.812	1.812		104.4			-0.797

[a] Fitted PES of UCCSD(T)-F12a/AVTZ, this work. [b] Fitted PES of UCCSD(T)-F12a/AVTZ, including spin-orbit coupling interaction, this work, [c] Fitted PES of UCCSD(T)-F12b/AVTZ, this work. [d] Fitted PES of UCCSD(T)-F12b/AVTZ, including spin-orbit coupling interaction, this work. [e]ZZGX PES. [f] UCCSD(T) -F12a/AVTZ, this work. [g] UCCSD(T) -F12b/AVTZ, this work.

Supplementary Table 2 Energies of the stationary points for the HCl + OH→Cl + H_2O reaction with respect to the OH + HCl asymptotic energy. Energies are in units of eV.

Method	RC(HO…HCl)	TS	PC(H_2O…Cl)	H_2O+Cl
F12a PES[a]	-0.155	0.088	-0.957	-0.800
F12a-so PES[b]	-0.148	0.095	-0.953	-0.826
F12b PES[c]	-0.154	0.097	-0.953	-0.796
F12b-so PES[d]	-0.147	0.104	-0.949	-0.822
ZZGX PES[e]	-0.152	0.095	-0.953	-0.794
UCCSD(T)-F12a[f]	-0.155	0.090	-0.957	-0.800
UCCSD(T)-F12b[g]	-0.155	0.096	-0.953	-0.797
AVTZ/UCCSD(T)	-0.157	0.104	-0.952	-0.809
AVQZ/UCCSD(T)	-0.155	0.100	-0.957	-0.807
AV5Z/UCCSD(T)	-0.153	0.107	-0.946	-0.793
CBS[h]	-0.150	0.113	-0.939	-0.784

a Fitted PES of UCCSD(T)-F12a/AVTZ, this work. b Fitted PES of UCCSD(T)-F12a/AVTZ, including spin-orbit coupling interaction, this work, c Fitted PES of UCCSD(T)-F12b/AVTZ, this work. d Fitted PES of UCCSD(T)-F12b/AVTZ, including spin-orbit coupling

$E_n^{Hartree-Fock} = A + B/C^n$

interaction, this work. e ZZGX PES. f UCCSD(T) -F12a/AVTZ, this work. g UCCSD(T) -F12b/AVTZ, this work. h For complete basis set (CBS) values, the Hartree Fock energies and correlations were extrapolated separately. A 3-parameter formula[20],

was used to extrapolate AV(T/Q/5)Z Hartree Fock energies to CBS, while for the electron correlation part, a 2-parameter formula[21] $E_n^{correlation} = A + B/n^3$ was used to extrapolate AVQZ and AV5Z energies.

Supplementary Table 3. Number of ab initio points, parameters of NN structures and fitting errors of the new Cl+H_2O PES

	Number of points	**NN structure**	**Fitting error (meV)**	
			F12a PES	**F12b PES**
1.HCl+OH	15809	7-30-30-1	1.3874	1.3068
2. Int(ClH….OH)	41612	7-60-60-1	4.0434	4.1508
3.Cl + H_2O	19995	7-30-30-1	0.9862	0.7646
In total	**70210**		**3.07**	**3.12**
Spin-Orbit	38000	7-20-20-1	0.19	0.19

Supplementary Table 4. Detail setup for the ring-polymer molecular dynamics (RPMD) calculations for the OH + HCl → H_2O + Cl reaction.

Parameter	**OH + HCl → H_2O + Cl**			**Explanation**
Command line parameters				
Temp	200	400	700	Temperature (K)
	250	500	1000	
	300			
N_{beads}	64	32	16	Number of beads
Dividing surface parameters				
R_∞	25			Dividing surface s1 parameters(a_0)
N_{bond}	1			Number of forming and breaking bonds
$N_{channel}$	1			Number of equivalent and product channels
Thermostat	“Andersen”			Thermostat option
Biased sampling parameters				
$N_{windows}$	111			Number of windows
ξ_1	-0.05			Center of the first window
$d\xi$	0.01			Window spacing step
ξ_N	1.05			Center of the last window
dt	0.0001			Time step (ps)
K_i	2.727			Umbrella force constant ((T/K)eV)
$N_{trajectory}$	100			Number of trajectories
$t_{equilibration}$	10			Equilibration period (ps)
$t_{sampling}$	50			Sampling period in each trajectory (ps)
N_i	5×10^7			Total number of sampling points
Potential of mean force calculation				

ξ_0	-0.02	Start of umbrella integration
ξt	1.05	End of umbrella integration
N_{bins}	5000	Number of bins
Recrossing factor calculation		
dt	0.0001	Time step (ps)
$t_{equilibration}$	20	Equilibration period (ps) in the constrained (parent) trajectory
$N_{totalchild}$	100 000	Total number of unconstrained (child) trajectory (ps)
$t_{childsampling}$	2	Sampling increment along the parent trajectory (ps)
N_{child}	100	Number of child trajectories per one initially constrained configuration
t_{child}	0.05	Length of child trajectories (ps)

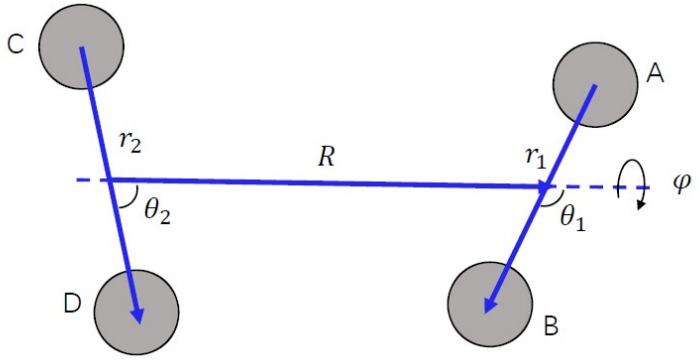

Supplementary Figure 1. The reagent Jacobi coordinates for AB+CD diatom-diatom arrangement.

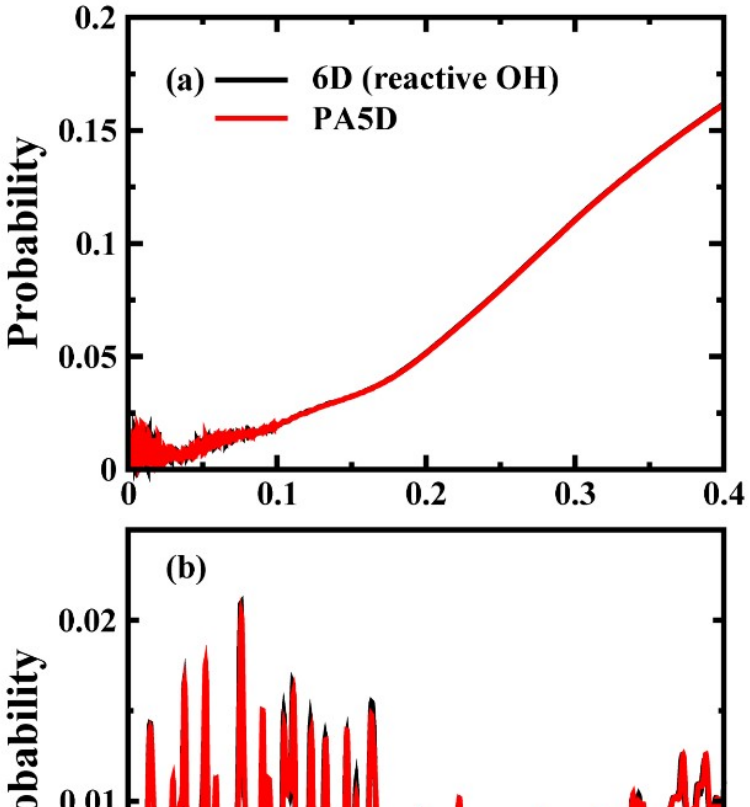

Supplementary Figure 2. The 6D and PA5D total reaction probabilities as a function of collision energy corresponding to the ground initial state at the propagation time of 550,000 a.u..

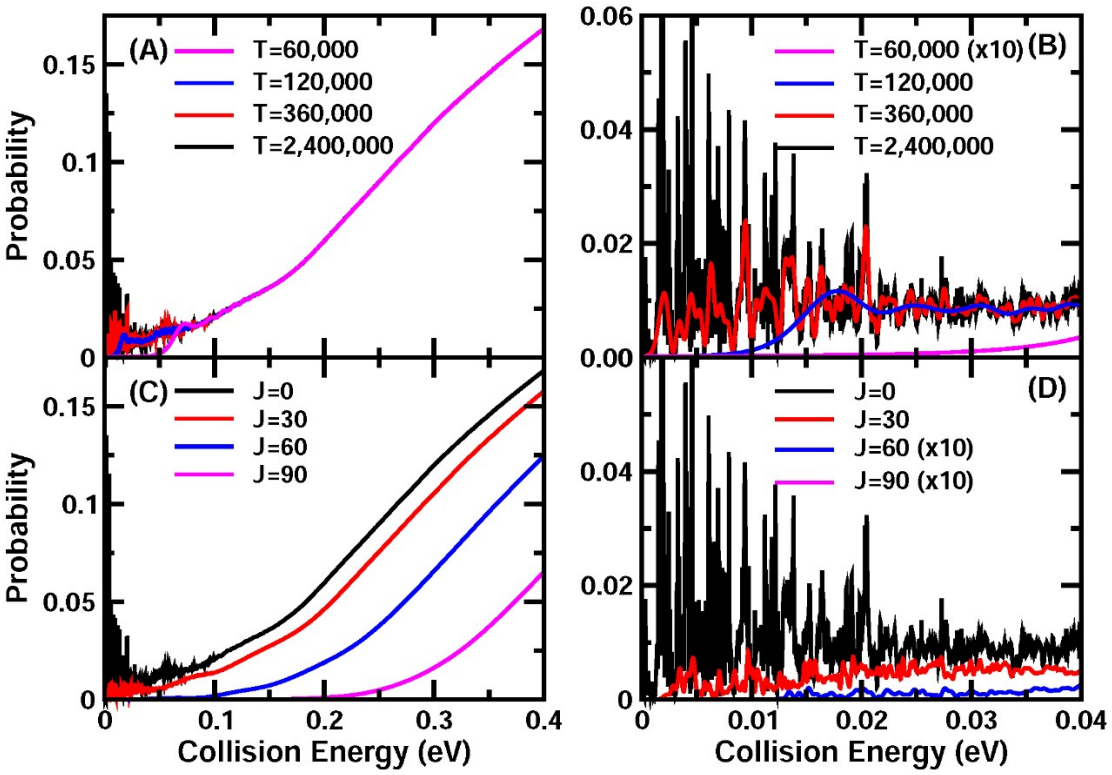

Supplementary Figure 3. (A) Total reaction probabilities for the ground initial state of the OH + HCl → Cl + H_2O reaction on the F12a PES at wave packet propagation time of T = 60,000, 120,000, 360,000, and 2,400,000 a.u. (B) The same as for (A) except for showing the collision energy between 0.0 and 0.04 eV. (C) Total reaction probabilities for some partial waves J=0, 30, 60, 90 as a function of the collision energy. (D) The same as for (C) except for showing the collision energy between 0.0 and 0.04 eV.

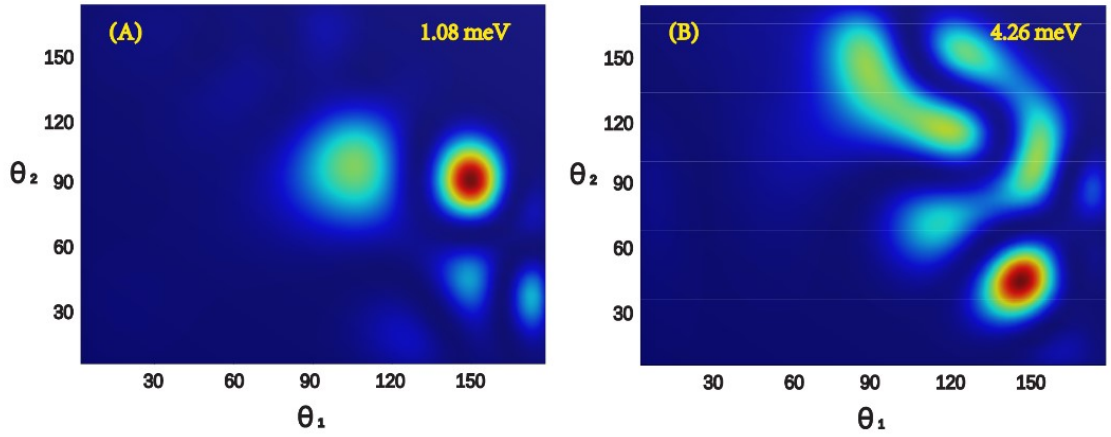

Supplementary Figure 4. Reactive scattering wave functions for the OH + HCl → Cl + H_2O reaction in the HCl bending coordinate (θ_1) and OH bending coordinates (θ_2) at the collision energies of 1.08 and 4.26 meV, with R, r_{HCl} and φ fixed at the peak position of 6.65, 2.43 and 0.06 a.u.. The coordinate units in the figures are degree.

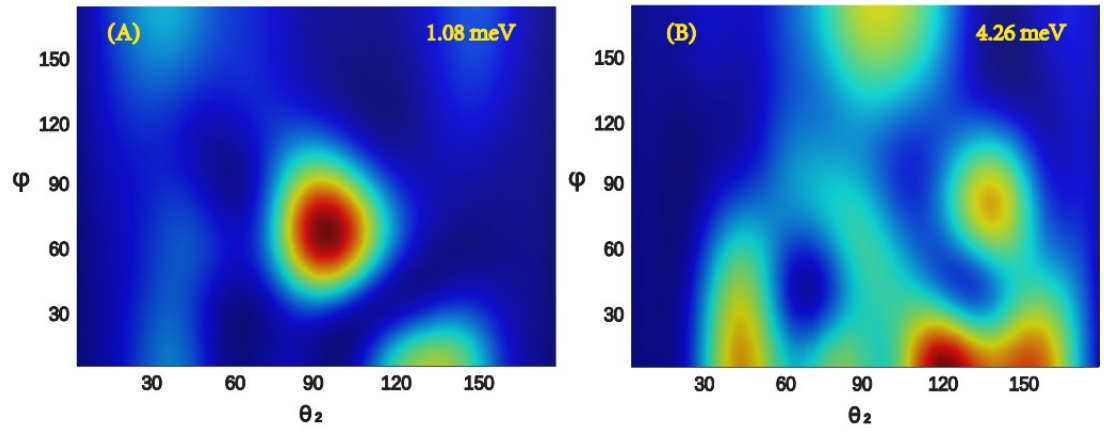

Supplementary Figure 5. Reactive scattering wave functions for the OH + HCl → Cl + H_2O reaction in the OH bending coordinate (θ_2) and the torsion coordinate (φ) at the collision energies of 1.08 and 4.26 meV, with R, r_{HCl} fixed at the peak position of 6.65, 2.43 a.u. and the HCl bending coordinate (θ_1) integrated. The coordinate units in the figures are degree.

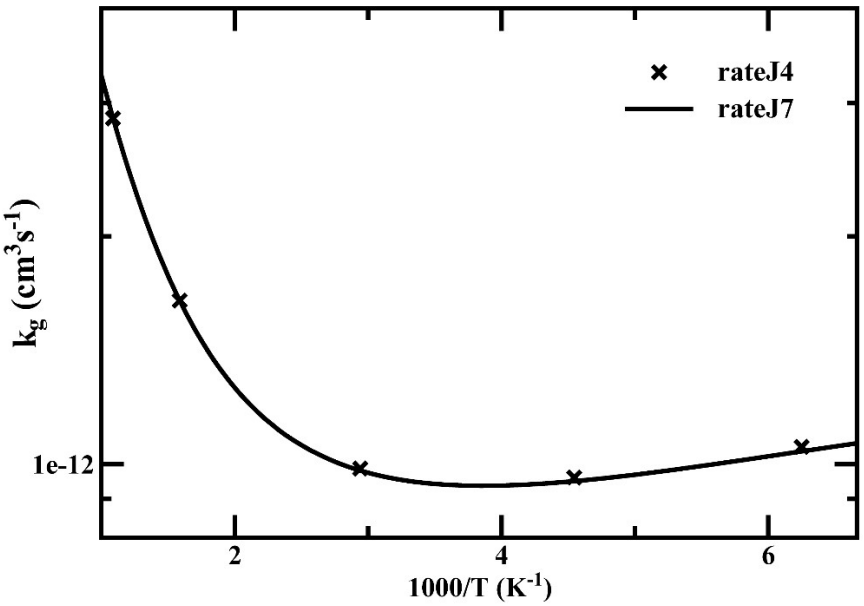

Supplementary Figure 6. Comparison of the rate constants for the initial ground rovibrational state of the HCl + OH → H_2O + Cl reaction calculated on F12b PES with *J*=0, 30, 60, 90 and *J*=0, 15, 30, 45, 60, 75, 90.

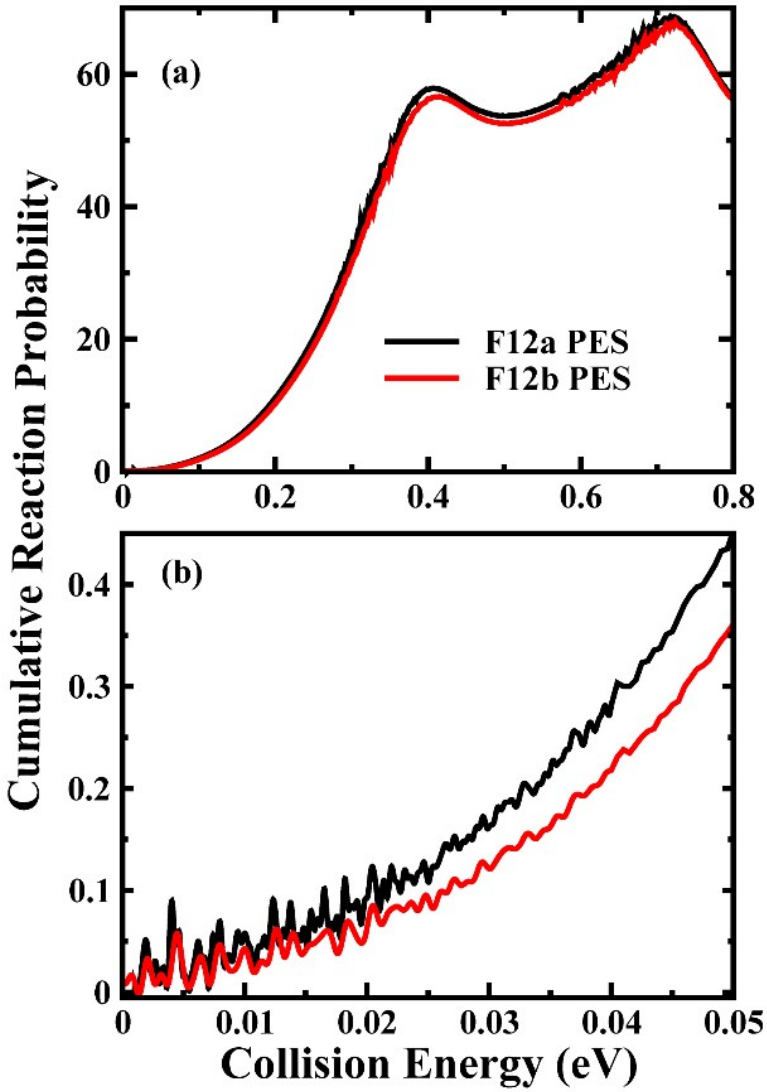

Supplementary Figure 7. (a) Cumulative reaction probability $N(E)$ as a function of total energy for the HCl + OH → H_2O + Cl reaction; (b) The same as for (a) except for showing the collision energy between 0.0 and 0.05 eV.

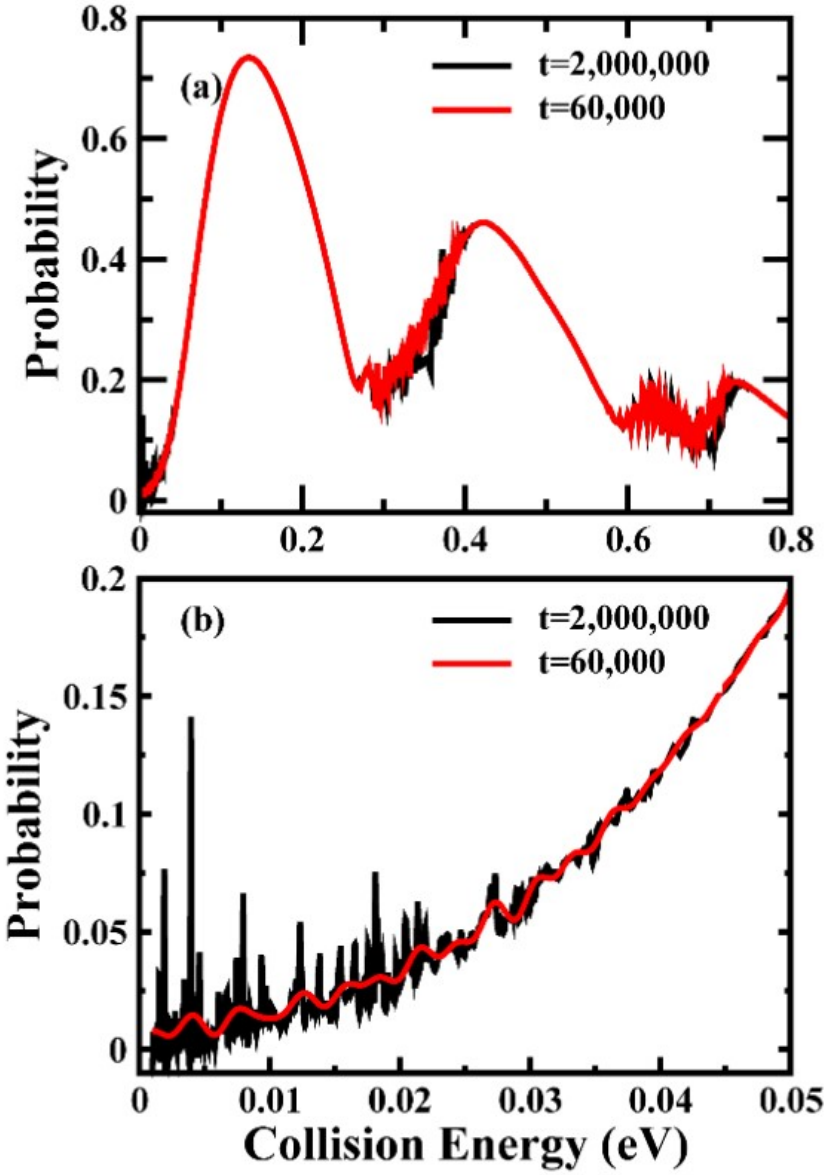

Supplementary Figure 8. (a) Cumulative reaction probability $N(E)$ of the partial waves J=0 as a function of total energy for the HCl + OH → H_2O + Cl reaction at wave packet propagation time of t=60,000 and 2,000,000 a.u.; (b) The same as for (a) except for showing the collision energy between 0.0 and 0.05 eV.

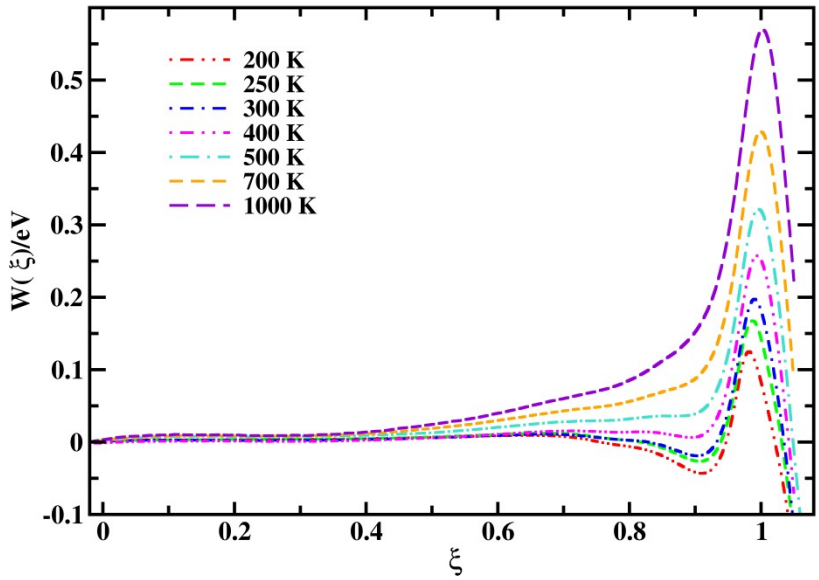

Supplementary Figure 9. Free-energy curves from RPMD simulations for the OH + HCl → H_2O + Cl reaction on the F12b PES at temperatures between 200 K and 1000 K.

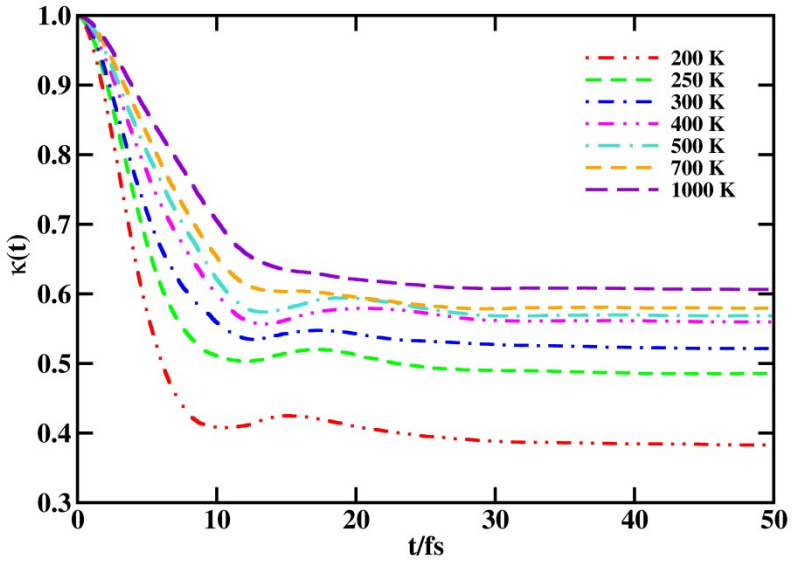

Supplementary Figure 10. RPMD transmission coefficients for the OH + HCl → H_2O + Cl reaction computed on the F12b PES at temperatures between 200 K and 1000 K.

Reference:

1 H. Fliegl, W. Klopper and C. Hattig, *J. Chem. Phys.*, 2005, **122**, 084107.

2 H.-J. Werner, G. Knizia, T. B. Adler and O. Marchetti, *Z. Phys. Chem.*, 2010, **224**, 493-511.

3 H.-J. Werner, P. J. Knowles, G. Knizia, F. R. Manby and M. Schuetz, *WIREs Comput. Mol. Sci.*, 2012, **2**, 242-253.

4 K. Shao, J. Chen, Z. Zhao and D. H. Zhang, *J. Chem. Phys.*, 2016, **145**, 071101.

5 J. Chen, X. Xu, X. Xu and D. H. Zhang, *J. Chem. Phys.*, 2013, **138**, 221104.

6 M. T. Hagan and M. B. Menhaj, *IEEE Trans. Neural Netw.*, 1994, **5**, 989-993.

7 W. Sarle, *Proceedings of the 27th Symposium on the Interface of Computing Science and Statistics*, 1995, 352-360.

8 D. H. Zhang and J. Z. H. Zhang, *J. Chem. Phys.*, 1994, **101**, 1146-1156.

9 J. M. Bowman, *J. Phys. Chem.*, 1991, **95**, 4960-4968.

10 D. H. Zhang and J. Z. H. Zhang, *J. Chem. Phys.*, 1994, **100**, 2697-2706.

11 D. H. Zhang and J. Z. H. Zhang, *J. Chem. Phys.*, 1999, **110**, 7622-7626.

12 D. H. Zhang and J. C. Light, *J. Chem. Phys.*, 1996, **104**, 6184-6191.

13 W. H. Miller, S. D. Schwartz and J. W. Tromp, *J. Chem. Phys.*, 1983, **79**, 4889-4898.

14 T. J. Park and J. C. Light, *J. Chem. Phys.*, 1986, **85**, 5870-5876.

15 T. J. Park and J. C. Light, *J. Chem. Phys.*, 1988, **88**, 4897-4912.

16 T. Seideman and W. H. Miller, *J. Chem. Phys.*, 1991, **95**, 1768-1780.

17 D. H. Zhang and J. C. Light, *J. Chem. Phys.*, 1997, **106**, 551-563.

18 D. C. Clary, *J. Chem. Phys.*, 1991, **95**, 7298-7310.

19 D. H. Zhang, J. Z. H. Zhang, Y. C. Zhang, D. Y. Wang and Q. G. Zhang, *J. Chem. Phys.*, 1995, **102**, 7400-7408.

20 D. Feller, *J. Chem. Phys.*, 1992, **96**, 6104-6114.

21 A. Halkier, T. Helgaker, P. Jørgensen, W. Klopper, H. Koch, J. Olsen and A. K. Wilson, *Chemical Physics Letters*, 1998, **286**, 243-252.